Digital Object Identifier 10.1109/APEC39645.2020.9124525

2020 IEEE Applied Power Electronics Conference and Exposition (APEC)

Multiwinding based Semi-Dual Active Bridge Converter

Felix Hoffmann

Jan-Ludwig Lafrenz

Marco Liserre

Nimrod Vazquez

Suggested Citation

F. Hoffmann, J. -L. Lafrenz, M. Liserre and N. Vazquez, "Multiwinding based Semi-Dual Active Bridge Converter," 2020 IEEE Applied Power Electronics Conference and Exposition (APEC), New Orleans, LA, USA, 2020.

Multiwinding based Semi-Dual Active Bridge Converter

Felix Hoffmann, *Student Member, IEEE*,
Jan-Ludwig Lafrenz, *Student Member, IEEE*,
Marco Liserre, *Fellow, IEEE*
Chair of Power Electronics
Christian-Albrechts-Universität zu Kiel
{fho,jll,ml}@tf.uni-kiel.de

Nimrod Vazquez, *Senior Member, IEEE*
Electrical and Electronics Departement
Tecnologico Nacional de Mexico /Instituto
Tecnologico de Celaya
Celaya, Mexico
n.vazquez@ieee.org

***Abstract*—Modular converter structures are state of the art for fast charging, since high power and short charging times are required. Multiwinding converter structures can bring several positive advantages, like cost and space reduction. However, the increased complexity due to the magnetically coupled ports needs to be handled. This paper introduces a multiwinding based Semidual-Active-Bridge converter with separated output voltages. The related design challenges in terms of independent charging voltage regulation are evaluated and design guidelines for the medium frequency transformer are presented. The theoretical analysis is validated experimentally.**

I. Introduction

Customers value the everyday applicability of electric vehicles (EVs) by the ease of the charging process. Therefore, the availability of chargers and charging duration are of paramount importance. In order to reduce the charging duration, level 3 DC fast charging stations (FCS) have been developed. In general, the basic structure of a FCS is shown in Fig. 1(a) and consists of a 50 Hz transformer which steps down the medium voltage (MV) to low voltage (LV). A central rectifier converts the LV-AC to LV DC, followed by a modular dc-dc stage, in which several isolated dc-dc converters are placed in parallel [1].

The dc-dc stage is a key component in FCS since it is responsible for isolation and voltage adaption. Especially, the wide output voltage range during the battery voltage charging process results in challenging requirements. In level 3 chargers, most of the energy is transferred in the constant current (CC) mode considering the CC-CV charging mode [2]. During the CC charging mode the output voltage of the dc-dc converter needs to change from the discharged battery voltage to the nominal battery voltage.

To meet the challenging requirements in terms of wide voltage range adaption and efficiency, the soft switched converter topologies are well suited as a building block [3]. The phase-shifted-full bridge (PSFB) is a widely used unidirectional topology [2]. The secondary side can be implemented with diode rectifier or an active rectifier. However inherently with the PSFB are the voltage spikes of the output diodes which require additional snubber circuits, reducing the efficiency of the converter [4]. Additionally , the large circulating currents and the loosing of ZVS at light loads are drawbacks of the PSFB [5].

In order to avoid the necessity for additional snubber circuits on the secondary side, a frequency controlled LLC converter is another solution [6] [7]. Especially operation points close to the resonant frequency lead to high efficiencies. However, the wide range of the battery voltage requires switching frequencies far away from the resonant frequency, reducing the converters efficiency. Additionally the filter design for a wide switching frequency range becomes more complex. This topology can be realized unidirectional or bidirectional.

Another widely used high efficient topology for battery charging is the dual active bridge (DAB). The DAB operates with a constant frequency and achieves ZVS conditions with a simple single phase shift (SPS) control [8] [9]. A phase shift between the primary and secondary side full bridges is applied, in order to control the power flow. Inherently with the DAB is the possibility of bidirectional operation. However, the feature of bidirectionality may not required for FCS and unidirectional power flow topologies are sufficient, since the main objective of FCS is to charge the vehicle as fast as possible, which excludes the necessity for vehicle to grid (V2G) operation. Replacing two secondary side switches with two diodes leads to the unidirectional semi-dual active bridge (semi-DAB) [10] [11]. The semi-DAB features the same positive characteristics like the DAB in terms of soft switching and high efficiency operation. At the same time the semi-DAB reduces the cost and the driver circuit complexity on the secondary side. Therefore, the semi-DAB is an excellent candidate as a building block for the dc-dc stage in FCS.

Apart from the conventional solutions for the isolated dc-dc converter with one input- and one output port (1 to 1), isolated multiport converters (x to x) are a promising solution. Potentials have been demonstrated in several application fields [12] [13] [14]. Especially, the 1x2 configuration reveals great potential for FCS. Two output ports are magnetically coupled with the input bridge by a multiwinding transformer (Fig.1(b)). This configuration reduces the number of necessary cells and leads to size and cost advantages, which is of particular interest

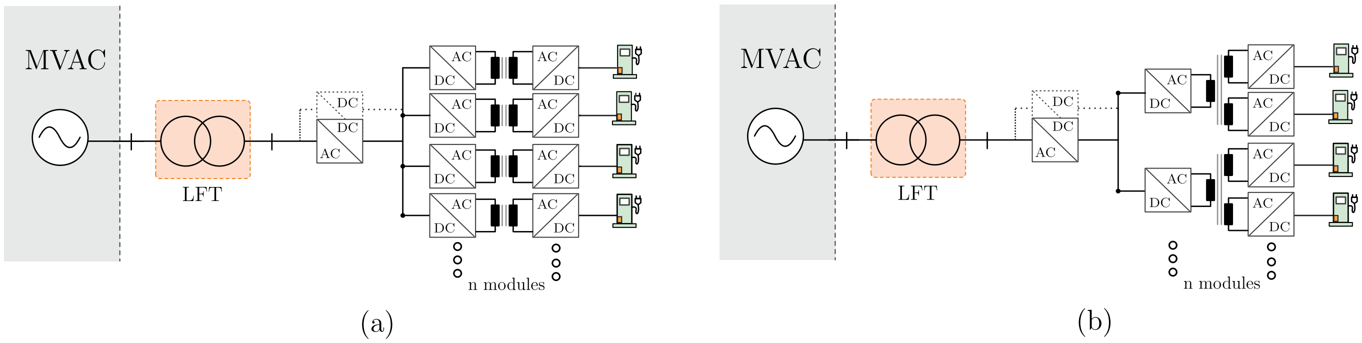

Figure 1. Fast charging station architectures; (a) Conventional solution with of the dc-dc stage [1], (b) Proposed solution with multiport converter (1x2) as basic building block for the dc-dc stage

from industry perspective. The realization of an unidirectional multiport converter structure with independently control of the output voltages requires a controllable rectifier. The semi-DAB meets these requirement for the proposed charging application. However, the combination of the wide output voltage range and the magnetic coupling of the output ports leads to certain design challenges for the semi-triple active bridge (semi-TAB) architecture.

Therefore, the paper proposes the MW semi-TAB converter and derives design challenges of the semi-TAB in MW configuration and present in particular the peculiarities of the medium frequency transformer (MFT) design. Section II describes the proposed ideal converter operation and derives requirements for decoupling the power flow. In Section III the effects of non-decoupled power flow are presented. Based on the previous analysis Section IV derives optimized design guidelines for the MFT design. The experimental verification is presented in Section V followed by the conclusion in Section VI.

II. Operation of Proposed semi-TAB with Seperated Outputs

The proposed converter consists of one full bridge inverter, a multiport MFT and the two secondary sides are composed by two semi active full bridge rectifiers with one switch and one diode leg (Fig.2(a)). Compared to the conventional investigated triple active-bridge (TAB) [15] [16], the total number of active devices is reduced by 4. Each bridge has an inductance in the MF AC-Link, which can be realized by the leakage inductance of the MFT or by external inductors.

All ports are operated with symmetrical square wave modulation. The input bridge voltage is fixed or used as reference. In order to regulate the output voltages, independent phase shift control is applied. An amplitude of nV_{in} is considered for the source (V_{T}), which is the reflected primary voltage to the secondary side of the transformer. This is valid under the assumption that $L_p \ll L_1 = L_2$; The voltages V_{T1} and V_{T2} have an amplitude of V_{C1} and V_{C2} respectively. Applying a phase shift (φ_1,φ_2), the effective voltage across the inductance L_1 and L_2 between the ports will change and the transferred power can be controlled. The idealized waveforms of the converter are shown in the Fig.2(b).

The operation principle can be divided into 5 states, which repeat with opposite sign in the next half period.

Period 1 ($t_o - t_1$):

In this period the primary side switches S_1 and S_4 are turned on and the primary transformer voltage v_p becomes V_{in}. The negative primary current i_{LP} starts to commutate. On the secondary side both switches S_5 and S_7 are on and the transformer secondary sides v_{T1} and v_{T2} are clamped to the negative output voltages V_{C1} and V_{C2}.

Period 2 ($t_1 - t_2$):

At the beginning of this period, the transformer current of the bridge with the larger phase shift φ_2 has reached the zero crossing. Hence the secondary side transformer voltage v_{T2} becomes zero. At the end of this period, the transformer current i_{L1} of the bridge with the smaller phase shift φ_1 has reached the zero crossing. Hence the secondary side transformer voltage v_{T1} becomes zero.

Period 3 ($t_2 - t_3$):

In this period, both secondary side transformer voltages v_{T1} and v_{T2} are zero. The primary side input voltage is shared among the inductances L_p, L_1 and L_2.

Period 4 ($t_3 - t_4$):

In the beginning of period the phase shift φ_1 is reached and the switch S_5 is turned off and S_6 is turned on. The transformer secondary side output voltage v_{T1} is clamped to the output voltage V_{C1}. At the end of this period, the phase shift φ_2 is reached and the switch S_7 is turned off and S_8 is turned on. The transformer secondary side output voltage v_{T2} is clamped to the output voltage V_{C2}.

Period 5 ($t_4 - t_5$):

In this period the primary side switches S_1 and S_4 are on. On the secondary side the power is transferred through the switches S_6 and S_8 and the diodes D_5 and D_7 are on.

Based on the waveforms, expressions for the currents can

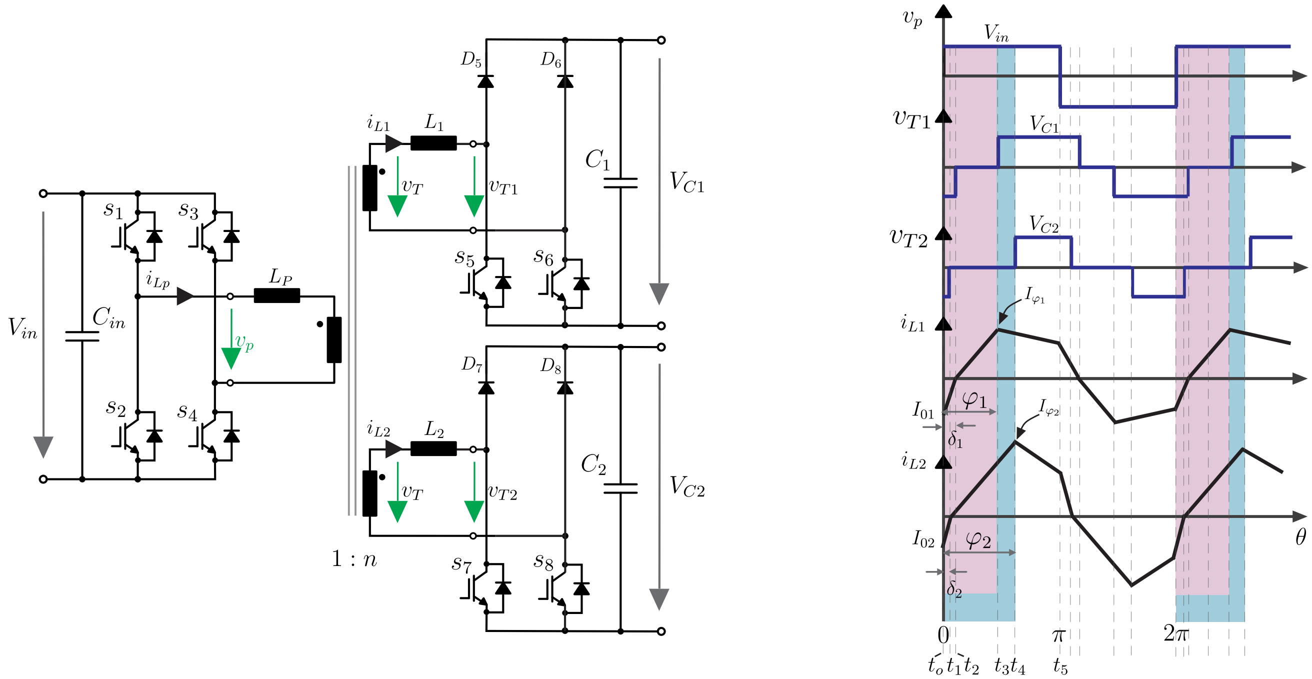

(a) (b)

Figure 2. (a) Investigated topology; semi-TAB with separated outputs forming the charging ports of an EV-charger, (b) Operation waveforms for decoupled outputs assuming $L_p \ll L_1 = L_2$

be derived :

$$i_{L1}(\theta) = \begin{cases} \dfrac{nV_{in} + V_{C1}}{\omega L_1}\theta - I_{01} & 0 \leq \theta \leq \delta_1 \\ \dfrac{nV_{in}}{\omega L_1}\theta & \delta_1 \leq \theta \leq \varphi_1 \\ \dfrac{nV_{in} - V_{C1}}{\omega L_1}\theta + I_{\varphi_1} & \varphi_1 \leq \theta \leq \pi \end{cases} \tag{1}$$

$$i_{L2}(\theta) = \begin{cases} \dfrac{nV_{in} + V_{C2}}{\omega L_2}\theta - I_{02} & 0 \leq \theta \leq \delta_2 \\ \dfrac{nV_{in}}{\omega L_2}\theta & \delta_2 \leq \theta \leq \varphi_2 \\ \dfrac{nV_{in} - V_{C2}}{\omega L_2}\theta + I_{\varphi_2} & \varphi_2 \leq \theta \leq \pi \end{cases} \tag{2}$$

I_{01}, I_{02}, $I_{\varphi 1}$ and $I_{\varphi 1}$ can be calculated as:

$$I_{\varphi_1} = \frac{V_{in}}{2\pi f_s L}(\varphi_1 - \delta) \tag{3}$$

$$I_{\pi} = \frac{V_{in} - V_{out}}{2\pi f_s L}(\pi - \varphi_1) + I_{\varphi_1} \tag{4}$$

With $I_\pi = I_0$ and inserting (3) in (5) follows for

$$I_0 = \frac{1}{1 + \frac{V_{in}}{V_{in} + V_{out}}}\left(\frac{V_{in}}{2\pi f_s L}\varphi + \frac{V_{in} - V_{out}}{2\pi f_s L}(\pi - \varphi_1)\right) \tag{5}$$

Equation (1) and (2) describing the current through the output bridges. Each output bridge of the MW SDAB is behaving like the conventional 1x1 SDAB described in [10]. For deriving the power transfer one half period is evaluated:

$$P_{1,2} = \frac{2V_{in}}{T_s}\int_0^{\pi} vp(t) i_L dt \tag{6}$$

With the previous derived expressions for the current follows:

$$P_{1,2} = \frac{V_{in}V_{out}A\varphi^2 + 4\pi B\varphi + \pi^2 C}{4\pi^2 f_s L (V_{out} + 2V_{in})^2} \tag{7}$$

With the constants: $A = V_{out} + 2V_{out}V_{in} + 2V_{in}^2$, $B = V_{out} + 2V_{out}V_{in} + V_{in}^2$ and $C = (2V_{out} + 2V_{in})(V_{in} - V_{out})$. Solving this equation to L leads to the required inductance between two bridges in order to achieve the desired power flow at a desired phase shift φ_{nom}.

In general three different operating modes for the semi-DAB are possible, which are also valid for the semi-TAB. The first mode is the standard operation mode which can occur in buck or boost mode (Fig.2(b)). Another operation mode can occur during buck mode. This mode occurs when the phase shift is small or the chosen bridge inductance is large. Operation mode 3 only occurs in boost mode. It is desired to operate the converter in mode 1 since the secondary side switches are loosing the ZVS range in mode 2 and mode 3 shows higher current stresses for the devices [11].

III. EFFECT OF NON-DECOUPLED OUTPUTS

The previous assumption $L_p \ll L_1 = L_2$ is difficult to realize, due to the leakage inductance of the primary side. Therefore, the design procedure becomes more challenging for the MW approach. Especially the choice of each external

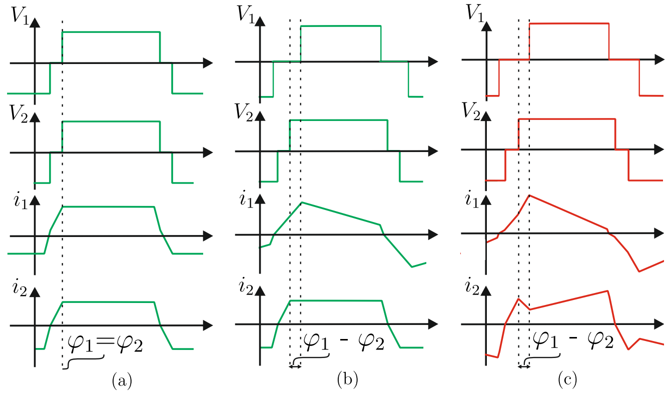

Figure 3. Effect of different inductance distribution between primary and secondary side (a) Symmetrical phase shift φ_1=φ_2 and hence no deviations in waveforms(b) Characteristic waveforms for $\varphi_1 \neq \varphi_2$ with $L_p \ll L_1 = L_2$ showing decoupling, (c) Characteristic waveforms for $\varphi_1 \neq \varphi_2$ with $L_p = L_1 = L_2$ showing coupling at output ports

bridge inductance is important in order to allow independent regulation of the output voltages (V_{C1},V_{C2}).

Fig 3 (a) shows a scenario in which both bridges have the same load requirement and hence φ_1=φ_2. The choice of the inductance ratio between secondary side inductance and primary side inductance $l_r = \frac{l_s}{l_p}$ has no influence on the waveforms.

However, for individual output voltages, the condition $\varphi_1 \neq \varphi_2$ is likely due to the different load requirements. As a consequence, a relative phase shift $\Delta\varphi = \varphi_1 - \varphi 2$ between the output bridges arises (Fig. 3(b)-(c)). Under this condition, the choice of the inductance ratio influences the behavior on the load regulation.

Fig 3 (b) shows the characteristic waveforms in case that φ_1 is increased and $L_p \ll L_1 = L_2$. It can be seen that changes of φ_1 have no effects on the current i_{L2} of bridge 2. The output ports are decoupled.

For the case that $L_p \ll L_1 = L_2$ is not fulfilled, changes in φ_1 influences the current i_{L2} of bridge 2 (Fig 3 (c)). A phase shift adaption of φ_2 is required in order to maintain the voltage constant, leading to higher current stresses on the devices, degrading the efficiency. The output ports are coupled.

The coupling effect during $\Delta\varphi$ depends on the l_r ratio. In the time interval from $t_2 - t_3$ (Fig. 2), both transformer output voltages are clamped to zero. The voltage across the inductances v_{L1} and v_{L2} in this period depends on the l_r ratio. The higher the l_r ratio, the higher the voltage across the secondary side inductances L_1 and L_2. The primary side input voltage is shared among the primary and secondary inductance as follows:

$$V_{in} = \frac{V_{LP}}{l_r} + \frac{V_{L2}}{2l_r} \tag{8}$$

After the bridge with the smaller phase shift has reached the phase shift φ_2, the voltage of V_{T2} is equal to the output voltage V_{C2} . V_1 is still zero. The current i_{L2} goes into buck mode operation (the output voltage is lower than the input voltage and a negative slop results), until the phase shift φ_1 of the other bridge is reached. In this period the voltage across each bridge inductance can be expressed as follows:

$$V_{LP} = \frac{V_{L1,2}}{l_r} \tag{9}$$

$$V_{L1} = V_{in} - \frac{V_{L2}}{l_r} \tag{10}$$

$$V_{L2} = -\frac{V_{L2}}{l_r} \tag{11}$$

The negative applied voltage across the inductance L_2 leads to the above described buck operation. It can be seen, that a higher l_r ratio leads to less negative voltage applied to L_2 in this period. This reduces the current dip shown in Fig. 3 (c) and hence the coupling effect between the two output ports.

In order to investigate the effect of different transformer inductance ratios, the output voltage V_{C1} of bridge 1 is increased to a desired level, while the output voltage V_{C2} of the other port should remain constant at a lower level. For this scenario a CC-CV charging curve is assumed (Fig. 4(a)), in which V_{C1} is located at the end of the CC-stage and V_{C2} at the beginning of the CC-stage. The evaluation is performed for different secondary ($L_S = L_1 = L_2$) to primary side inductance ratios ($l_r = \frac{L_S}{L_P}$), while the total inductance for all cases is the same. The simulation parameters are shown in table I. Fig. 4(b)-(d) show the current waveforms for the investigated cases. The higher the l_r ratio, the better is the decoupling between the two output bridges. Furthermore, it can be seen that for smaller values of l_r the current of the bridge with the higher phase shift (φ_1) goes into DCM operation.

For a more general consideration, Figure 5(a) and (b) show the required phase shifts for φ_1 and φ_2 in order to achieve a desired voltage difference $\Delta V = V_{C1} - V_{C2}$ of the two output ports in dependency of different l_r ratios. The total range of ΔV is derived from the CC-CV charging curve (Fig. 4(a)) for the worst case scenario, in which V_{C1} is located at the end of the CC-Stage and V_{C2} at the beginning of the CC-Stage. Based

Table I
SIMULATION SPECIFICATIONS

Input voltage	$V_{in} = 300$ V
Output voltage 1	$V_{C1} = [300, 310, \ldots 400]$ V
Output voltage 2	$V_{C2} = 300$ V
Charger Power	P_{unit} = 20 kW
Switching frequency	$f_s = 20$ kHz
Nominal PS angle	$\varphi_{nom} = 30°$
Transformer turns ratio	$n = 1$
Inductance ratio Scenario 1	l_r = 0.5
Inductance ratio Scenario 2	l_r = 1
Inductance ratio Scenario 3	l_r = 10

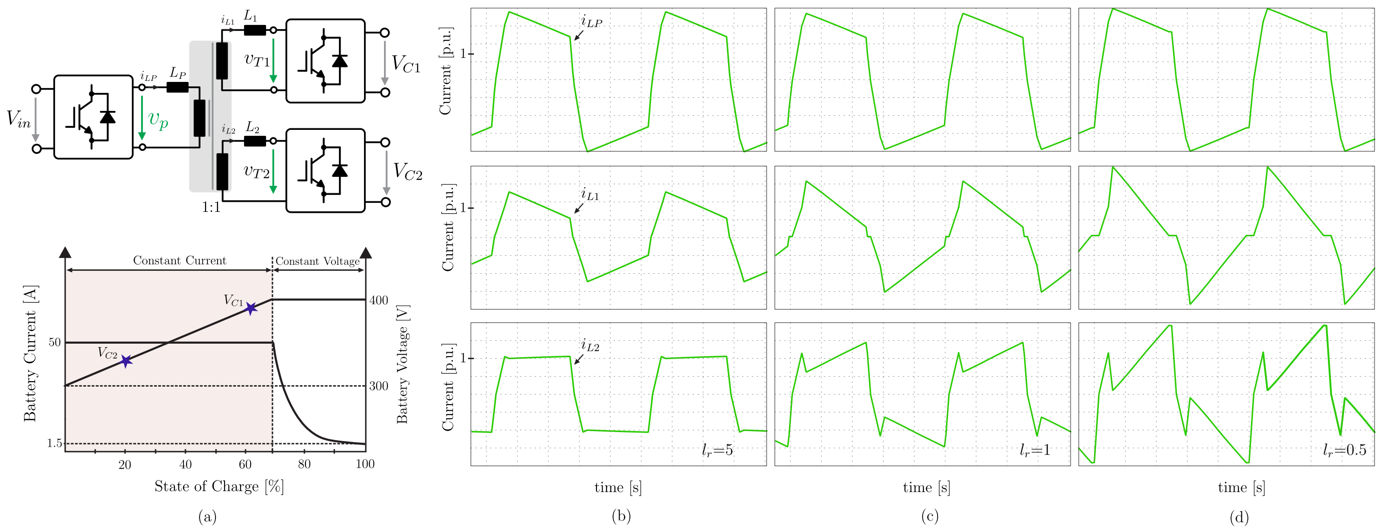

Figure 4. (a) Topology with SoC curve showing investigated operation points on charging curve for both outputs; Simulated normalized transformer current waveforms for different l_r ratios (Order from top: Pri. transformer current i_{Lp}, Sec. 1 transformer current i_{L1}, Sec. 2 transformer current i_{L2}): (b) $l_r = 5$ (c), $l_r = 1$, (d) $l_r = 0.5$

on equation (7), the nominal phase shift for $V_{C1} = V_{C2} = 320V$ and hence $\Delta V = 0$ is designed to be $\varphi_{1nom} = \varphi_{2nom} = 30°$.

It can be seen that the lower the $l_r = \frac{L_S}{L_P}$ ratio, the higher are the required phase shifts φ_1 and φ_2 for both bridges. Only large $l_r$inductance ratios lead to almost decoupled outputs. For example a l_r value of $l_r = 10$ leads only to a minimal required phase shift increase of φ2 from $\varphi_2 = 30°$ to $\varphi_2 = 32°$ in order to maintain $V_{C2} = 300V$ while V_{C1} is increased to $V_{C1} = 400V$. Fig. 5 shows the sum of the transformer winding rms currents in dependency for the voltage difference $\Delta V = V_{C1} - V_{C2}$ of the two output ports. The higher current stresses can be explained by the higher required phase shifts for small values of l_r. Furthermore the above described operation in DCM-mode for small l_r values lead to higher current stresses on the components, which reduces the efficiency of the semi-TAB.

From the analysis, it can be concluded that a higher l_r ratio between secondary and primary side inductance is beneficial for decoupling the output ports. As a consequence the current stresses on the components are reduced and hence the converter efficiency is increased. However, in order to reach the desired l_r ratio, additional external inductances are required, which increase the sum of total inductance in the circuit. From equation (7) it can be seen that a larger total inductance requires a higher nominal phase shift which leads to higher current stresses on the devices.

The higher the total leakage inductance, the less beneficial becomes a high l_r ratio, since the positive effects of the decoupling are compensated by the higher reactive currents due to the high value of inductance in the circuit. For small values of transformer inductance, the efficiency can be increased by realizing a high l_r ratio.

The trade-off between reduced current stresses for the decoupled case with a high l_r ratio and the higher current stresses due to higher values of external inductance for reaching the

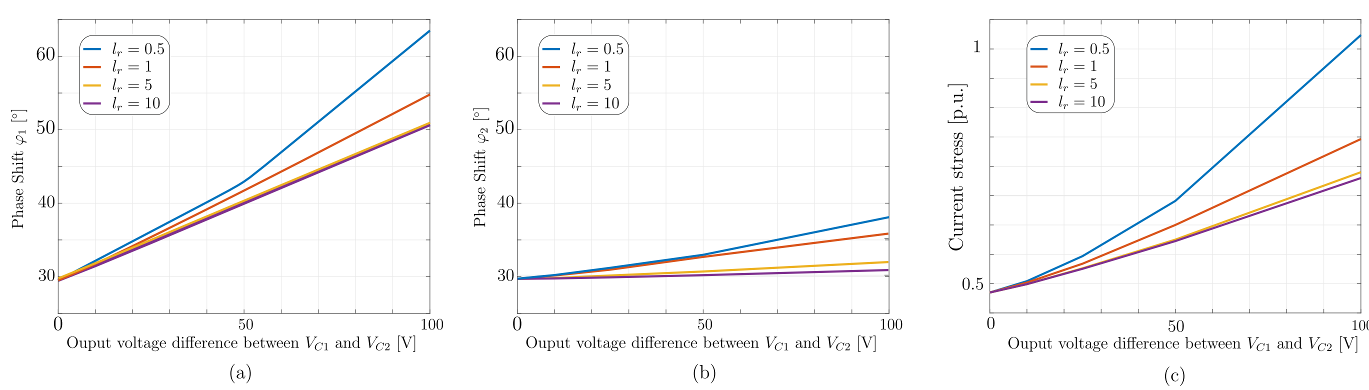

Figure 5. Effect of different l_r ratios on the required phase shift for different voltages at the output ports and resulting current stresses. V_{C1} is increased from 300V to 400V while V_{C2} is kept constant at $V_{C2} = 300V$; (a) Required phase shift φ_1, (b) Required phase shift φ_2, (c) Normalized sum of the rms currents through the transformer windings

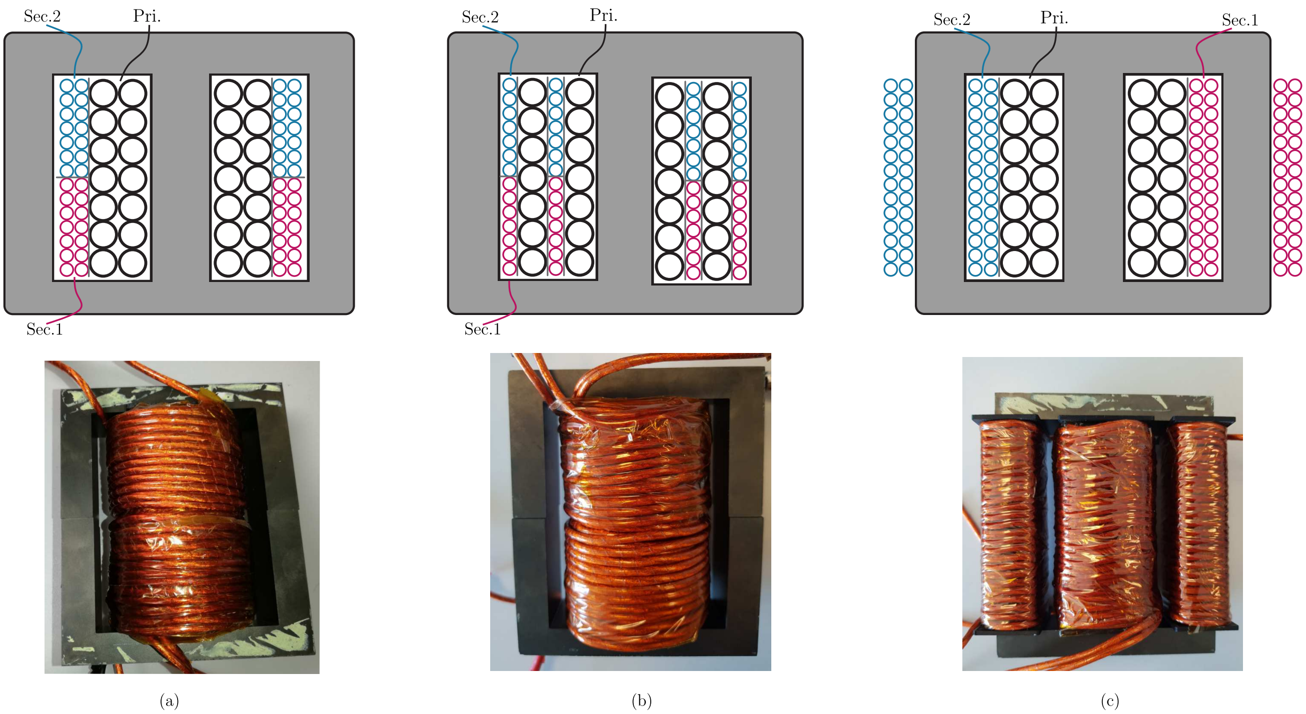

Figure 6. Different investigated transformer winding structures with E-Core and practical realization; (a) stacked structure , (b) interleaved stacked structure, (c) separated structure

desired l_r ratio needs to be considered when designing the MFT.

IV. MAGNETIC DESIGN CONSIDERATION

The previous analysis revealed that a high ratio between secondary and primary inductance is beneficial for the proposed topology in terms of independent output voltage regulation and current stresses. Additionally, the total inductance should not be too large in order to avoid unnecessary reactive currents, which downsizes the efficiency. The total inductance in each port is the sum of external inductance and leakage inductance by the MFT. Selecting a proper transformer design enables the realization of a high l_r ration, while minimizing the required external inductance. The leakage inductance of a MFT depends on the winding architecture and in particular on the distance between the windings [17].

One commonly used winding structure is the layered structure, in which the primary winding is followed by the first secondary winding and afterward by the second secondary winding. However, this structure is not further considered because of the deviations between L_1 and L_2.

Three possible winding structures (Fig. 6(a)-(c)) are investigated, in order to achieve decoupling between the secondary side windings. The first one is a stacked configuration (Fig. 6(a)), in which the secondary side windings have a stacked arrangement above the primary winding. Interleaving the windigs of the stacked configuration leads to the second configuration (Fig. 6(b)). In general interleaving the windings improves further the primary to secondary side coupling, which reduces the total leakage inductance. Another possible configuration is the separate winding structure (Fig. 6(c)). Each winding is wound on separately on the limbs of the E-core. The maximum distance between the two secondary windings ensures high values of L_1 and L_2.

Modeling the three port MFT with the commonly used T-model can lead to negative values for the leakage inductance while extracting the parameters from terminal measurement [17]. Although the model represents the system in a correct way [18], it is not convenient to make any statements about the suitability of the investigated winding configuration. Therefore, the rating is based on the coupling factors $k_p = k_{12} \approx k_{13}$, $k_s = k_{23}$ and the total inductance L_{PSC} seen by the primary side during a short circuit of the output windings.

$$k_p = \sqrt{1 - \frac{L_{LK12}}{L_{11}}} \approx \sqrt{1 - \frac{L_{LK13}}{L_{11}}} \tag{12}$$

$$k_s = \sqrt{1 - \frac{L_{LK23}}{L_{22}}} \approx \sqrt{1 - \frac{L_{LK23}}{L_{33}}} \tag{13}$$

Where L_{LK12}, L_{LK13} and L_{LK23} represents the measured leakage inductance between each of the bridges. L_{11} represent the primary self inductance, L_{22} and L_{33} the secondary.

Based on the terminal measurement (Table 1), it can be seen that the separated structure shows the lowest coupling of the secondary sides. However, the low value of k_p indicates a high total leakage inductance L_{PSC}, which would lead to higher required phase shifts. The interleaved stacked configuration (Fig. 6(c)) is most promising due to the low coupling k_s of the secondary while minimizing the total leakage inductance L_{PSC}.

Table II
DIFFERENT INVESTIGATED WINDING STRUCTURES

	Stacked	Interleaved Stacked	Separated
$L_{PSC}[\mu H]$	12	4	123
k_P	0.93	0.95	0.43
k_S	0.8	0.81	0.36

V. EXPERIMENTAL RESULTS

Fig. 7(a) shows the lab set up and the specifications are given in table III. Basic waveforms of the semi-TAB without differences in the output voltage are shown in Fig 7(b). The transformer output voltages V_{T1} and V_{T2} are equal. In order to prove the influence of the inductance ratio l_r on the coupling of the output ports, different inductance ratios l_r have been tested with the stacked interleaved winding configuration. Based on the results on the analysis of Section IV, additional external inductance have been added to reach the desired l_r ratios. In the following the output voltage V_{T1} of port one

Table III
EXPERIMENTAL SPECIFICATIONS

Input voltage	$V_{in} = 250$ V
Output voltage 1	$V_{C1} = [250, 310, ...350]$ V
Output voltage 2	$V_{C2} = 250$ V
Switching frequency	$f_s = 20$ kHz
Nominal PS angle	$\varphi_{nom} = 30°$
Transformer turns ratio	$n = 1$
Primary side switches	C2M0025120D
Secondary side switches	C2M0040120D
Secodary side diodes	C4D40120D

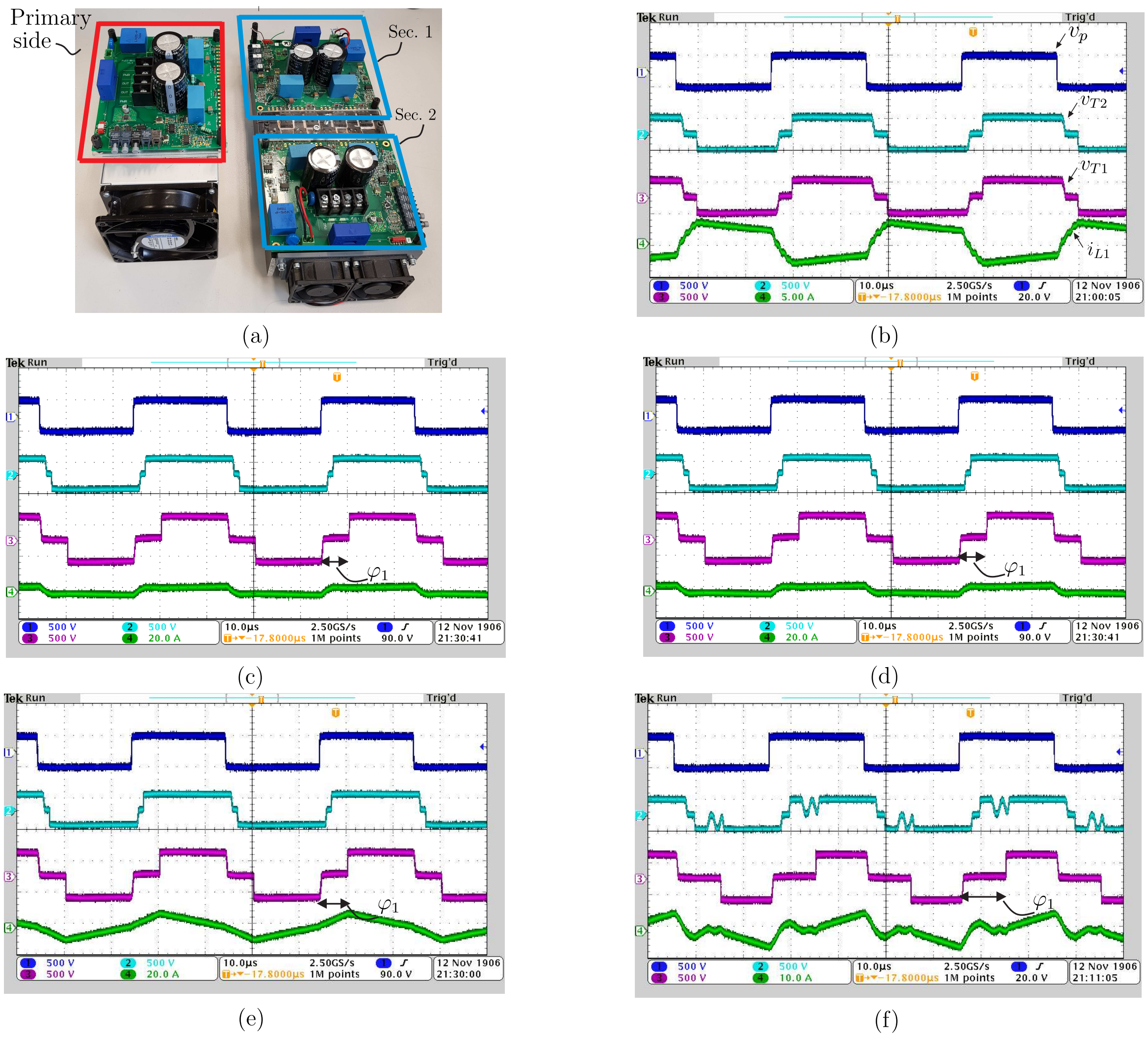

Figure 7. Experimental verification and investigation of different operating modes of semi-TAB depending on l_r ratio, realized with interleaved stacked structure:(a) Primary side and secondary side bridges, (b) semi-TAB operation with same output voltages; Output voltage V_{T1} of port 1 is increased for different l_r (c)$l_r = 5$ CCM, (d) $l_r = 2$ CCM, (e) $l_r = 1$ Boundary mode (f) $l_r = 0.5$ DCM operation (blue curve: Pri. transformer voltage, light blue curve: Sec. transformer voltage of port 2, pink curve: Sec. transformer voltage of port 1, green curve: Transformer current of port 1)

is increased from 250V to 350V while the voltage V_{T2} of the other port is kept constant. Fig.7 (c) shows the case for a nearly decoupled case ($l_r = 5$). Reducing the ratios show higher couplings between the output ports (Fig. 7(d)-(f)). Therefore the phase shift φ_1 and φ_2 needs to be increased. In Fig. 7(f) the low inductance ratio $l_r = 0.5$ leads to DCM operation. This complies with the theoretical analysis in Fig. 4. The ringing of the transformer output voltage V_{T2} during the zero current interval is due to the output capacitance of the devices which resonate with the leakage inductance of the transformer [11].

VI. Conclusion

The paper introduced the semi-TAB topology as a promising architecture for the dc-dc stage of a FCS. It has been shown that for the semi-TAB, the transformer design is of crucial importance. The ratio between the secondary and primary inductance should be large in order to avoid circulating current for different load conditions in the output bridges. However, the total external inductance should not be to high, since it increases the required phase shifts (φ_1, φ_2) and therefore the reactive power flow. Hence a transformer winding architecture which increases l_r ratio while at the same time minimizing the total leakage inductance is the preferred structure for the considered application field. Especially the interleaved stacked winding structure fulfills this target. Different operation modes, depending on the l_r ratio have been derived and experimentally validated.

VII. Acknowledgment

’This work was supported in part by the European Union/Interreg V-A - Germany-Denmark, under the PE:Region Project and in part by the European Research Council under the European Unions Seventh Framework Programme (FP/2007-2013)/ERC Grant 616344-HEART.

References

[1] Enercon e-charger 600 leaflet. [Online]. Available: https://www.enercon.de/fileadmin/Redakteur/Service/EC_E-Charger_600_en_web.pdf

[2] P. K. Prasobhu, F. Hoffmann, and M. Liserre, “Optimal trade-off between hard and soft-switching to achieve energy saving in industrial electric vehicles,” in *IECON 2018 - 44th Annual Conference of the IEEE Industrial Electronics Society*, Oct 2018, pp. 2116–2121.

[3] M. Yilmaz and P. T. Krein, “Review of battery charger topologies, charging power levels, and infrastructure for plug-in electric and hybrid vehicles,” *IEEE Transactions on Power Electronics*, vol. 28, no. 5, pp. 2151–2169, May 2013.

[7] H. Wang, S. Dusmez, and A. Khaligh, “Design and analysis of a full-bridge llc-based pev charger optimized for wide battery voltage range,” *IEEE Transactions on Vehicular Technology*, vol. 63, no. 4, pp. 1603–1613, May 2014.

[4] Y. Lo, C. Lin, M. Hsieh, and C. Lin, “Phase-shifted full-bridge series-resonant dc-dc converters for wide load variations,” *IEEE Transactions on Industrial Electronics*, vol. 58, no. 6, pp. 2572–2575, June 2011.

[5] D. Sha, K. Deng, and X. Liao, “Duty cycle exchanging control for input-series-output-series connected two ps-fb dc-dc converters,” *IEEE Transactions on Power Electronics*, vol. 27, no. 3, pp. 1490–1501, March 2012.

[6] J. Deng, S. Li, S. Hu, C. C. Mi, and R. Ma, “Design methodology of llc resonant converters for electric vehicle battery chargers,” *IEEE Transactions on Vehicular Technology*, vol. 63, no. 4, pp. 1581–1592, May 2014.

[8] L. Xue, D. Boroyevich, and P. Mattavelli, “Switching condition and loss modeling of gan-based dual active bridge converter for phev charger,” in *2016 IEEE Applied Power Electronics Conference and Exposition (APEC)*, March 2016, pp. 1315–1322.

[9] S. Inoue and H. Akagi, “A bidirectional dcdc converter for an energy storage system with galvanic isolation,” *IEEE Transactions on Power Electronics*, vol. 22, no. 6, pp. 2299–2306, Nov 2007.

[10] S. Kulasekaran and R. Ayyanar, “Analysis, design, and experimental results of the semidual-active-bridge converter,” *IEEE Transactions on Power Electronics*, vol. 29, no. 10, pp. 5136–5147, Oct 2014.

[11] M. Lu, S. Hu, S. Zhou, Y. Tang, and X. Li, “The steady-state operation map of a semi-dual-active-bridge converter,” in *2017 12th IEEE Conference on Industrial Electronics and Applications (ICIEA)*, June 2017, pp. 1586–1590.

[12] R. Kasashima, S. Nakagawa, K. Nishimoto, Y. Kado, and K. Wada, “Power loss analysis of 10kw three-way isolated dc/dc converter using sic-mosfets as a power routing unit for constructing 400v dc microgrid systems,” in *IECON 2016 - 42nd Annual Conference of the IEEE Industrial Electronics Society*, Oct 2016, pp. 1394–1399.

[13] Savitha K.P and P. Kanakasabapathy, “Multi-port dc-dc converter for dc microgrid applications,” in *2016 IEEE 6th International Conference on Power Systems (ICPS)*, March 2016, pp. 1–6.

[14] K. Venugopal and P. Kanakasabapathy, “Three port multi winding flyback converter for dc microgrid applications,” in *2017 International Conference on Technological Advancements in Power and Energy (TAP Energy)*, Dec 2017, pp. 1–6.

[15] R. Chattopadhyay, G. Gohil, S. Acharya, V. Nair, and S. Bhattacharya, “Efficiency improvement of three port high frequency transformer isolated triple active bridge converter,” in *2018 IEEE Applied Power Electronics Conference and Exposition (APEC)*, March 2018, pp. 1807–1814.

[16] and K. Masumoto, K. Wada, and Y. Kado, “Power flow control of a triple active bridge dc-dc converter using gan power devices for a low-voltage dc power distribution system,” in *2017 IEEE 3rd International Future Energy Electronics Conference and ECCE Asia (IFEEC 2017 - ECCE Asia)*, June 2017, pp. 772–777.

[17] Qing Chen, F. C. Lee, Jian Zhong Jiang, and M. M. Jovanovic, “A new model for multiple-winding transformer,” in *Proceedings of 1994 Power Electronics Specialist Conference - PESC’94*, vol. 2, June 1994, pp. 864–871 vol.2.

[18] M. Albach, *Induktivitaeten in der Leistungselektronik: Spulen, Trafos und ihre parasitaeren Eigenschaften (German Edition)*. Springer Vieweg, 2017.